PHYSICAL REVIEW FLUIDS **4**, 021101(R) (2019)

Rapid Communications

Transition in swimming direction in a model self-propelled inertial swimmer

Thomas Dombrowski,[1,*] Shannon K. Jones,[2,*] Georgios Katsikis,[3] Amneet Pal Singh Bhalla,[4] Boyce E. Griffith,[2,5,6] and Daphne Klotsa[2,†]

[1]*Department of Physics, The University of North Carolina at Chapel Hill, Chapel Hill, North Carolina 27599, USA*

[2]*Department of Applied Physical Sciences, The University of North Carolina at Chapel Hill, Chapel Hill, North Carolina 27599, USA*

[3]*Koch Institute for Integrative Cancer Research, Massachusetts Institute of Technology, Cambridge, Massachusetts 02139, USA*

[4]*Mechanical Engineering, San Diego State University, California 92182, USA*

[5]*Department of Mathematics, The University of North Carolina at Chapel Hill, Chapel Hill, North Carolina 27599, USA*

[6]*Department of Biomedical Engineering, The University of North Carolina at Chapel Hill, Chapel Hill, North Carolina 27599, USA*

(Received 23 December 2017; revised manuscript received 28 August 2018; published 8 February 2019)

We propose a reciprocal, self-propelled model swimmer at intermediate Reynolds numbers (Re). Our swimmer consists of two unequal spheres that oscillate in antiphase, generating nonlinear steady streaming (SS) flows. We show computationally that the SS flows enable the swimmer to propel itself, and also switch direction as Re increases. We quantify the transition in the swimming direction by collapsing our data on a critical Re and show that the transition in swimming directions corresponds to the reversal of the SS flows. Based on our findings, we propose that SS can be an important physical mechanism for motility at intermediate Re.

DOI: 10.1103/PhysRevFluids.4.021101

Understanding motility requires connections between fundamental physics and biology [1–3] and has many applications, including drug-delivering nanomachines [4,5] and autonomous underwater vehicles [6–8]. Swimming regimes can be classified by the Reynolds number (Re), which characterizes the relative importance of inertial over viscous forces. Although there is a large body of work on motility in Stokes flows ($\mathrm{Re} \ll 1$), in which viscous forces dominate, and at high Re ($\mathrm{Re} \gg 1$), in which inertial forces dominate, less is known about the intermediate regime $\mathrm{Re}_{\mathrm{int}} \sim 1$–1000 [2,9,10].

The $\mathrm{Re}_{\mathrm{int}}$ regime encompasses an enormous diversity of organisms, ranging from larvae (of, e.g., fish, squid, ascidian) and large ciliates, to nematodes, copepods, plankton, and jellyfish. These swimmers employ a variety of motility mechanisms: jet propulsion [11,12], anguilliform locomotion [13–17], rowing [18,19], aquatic flapping flight [20], and ciliate beating [21,22]. Plankton have even been proposed to contribute to the large-scale transport of nutrients and dissolved gases in the ocean [23–27]. However, most prior studies on $\mathrm{Re}_{\mathrm{int}}$ motility have focused on the details of specific organisms [11–14,16–22,24,25,28]. As a result, few general models exist for

*These authors contributed equally to this work.
†dklotsa@email.unc.edu

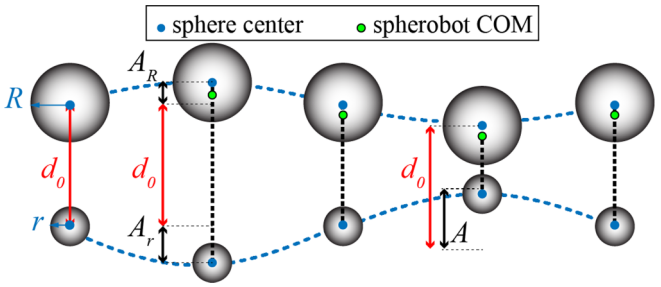

FIG. 1. Reciprocal oscillation of the spherobot swimmer over one cycle. Spheres' centers of mass (COM) (blue circles) and the spherobot COM (green circle) are indicated. The distance between the spheres' centers $d(t)$ is d_0 at the equilibrium distance, $d_0 - A$ at minimum distance, and $d_0 + A$ at maximum distance. The total amplitude is $A = A_R + A_r$.

motility at $\mathrm{Re_{int}}$; examples are an extension of the Stokesian squirmer to include inertia [27,29–33], which makes assumptions about the generation of flow due to small-amplitude oscillations on the surface of a spherical swimmer and the flapping-plate model, which is a lumped-torsional-flexibility model that uses passive pitching and responds to an actuation [34,35]. Still, there is a lack of understanding regarding the unifying physical mechanisms that swimmers at $\mathrm{Re_{int}}$ exhibit. To develop a theoretical basis for swimming, more models with varying degrees of freedom that operate under different conditions at $\mathrm{Re_{int}}$ are needed. Only then can we make progress in better understanding biological swimmers and designing artificial ones at intermediate scales.

Steady streaming (SS) is the nonzero, time-averaged flow that arises at $\mathrm{Re_{int}}$ due to oscillations of a rigid body in a fluid and has been studied for various cases, such as around a single sphere [36–40], cylinder, near a wall. While SS has been used to manipulate particles [41–45] and cells [46] via *external* vibrations, it has not been used as a mechanism for self-propulsion, even though there have been suggestions that it may be relevant for the enhanced motility of *Synechococcus* cyanobacteria [47].

In this Rapid Communication, we propose a simple, reciprocal and self-propelled model swimmer, termed the *spherobot*, that uses steady streaming flows for propulsion. The spherobot is composed of two unequal spheres that oscillate with respect to each other, in antiphase, generating SS flows [Fig. 1(a)]. We computationally studied the spherobot's motility over a broad range of parameters: viscosity, sphere amplitudes, distance between the spheres, sphere radii, and sphere-radii ratio. At $\mathrm{Re} = 0$, the spherobot cannot swim because of Purcell's scallop theorem [48]: its reciprocal stroke does not break time-reversal symmetry. At low, nonzero Re the spherobot started to swim and, interestingly, switched swimming direction from a small-sphere-leading to a large-sphere-leading regime. We found that the point of transition collapsed to a critical value when the appropriate Reynolds number was used, which revealed a strong dependence on the SS flows of the small sphere. Analyzing the flow fields, we showed that the transition in swimming direction corresponds to the reversal of SS flows around the spherobot that occurs as the Reynolds number increases.

Methods. The spherobot was composed of two unequal spheres with radii r, R, which were coupled to one another by prescribing the distance between their centers. To model this computationally, we tethered the two spheres using an active spring with a time-dependent resting length $d(t) = d_0 + A\sin(\omega t)$, in which d_0 is the equilibrium distance between the sphere centers, $A = 0.5(d_{\max} - d_{\min})$ is the amplitude of the spherobot, and ω is the frequency of oscillation (Fig. 1). Equal and opposite (spring) forces were applied to the spheres that acted to keep them approximately at the prescribed distance apart (error $\approx 10^{-7}$ m). Thus, the model ensures a geometrically reciprocal cycle and an internally-vibrated swimmer (no applied external fields or forces). Because the same force is applied to both spheres, the one with the smaller mass (the small

sphere) will have a larger amplitude A_r than the one with the bigger mass (large sphere), A_R (i.e., if $r \leqslant R$ then $A_r \geqslant A_R$). In most simulations we have $A_r \approx 4A_R$. The amplitude of the spherobot A is the sum of the two, $A = A_r + A_R$ (Fig. 1). Both spheres were neutrally buoyant with respect to the surrounding fluid. To simulate the spherobot in a fluid, we used an exactly constrained immersed boundary (CIB) method [49,50]. The CIB scheme is implemented in IBAMR [51,52], which provides several variants of the immersed boundary (IB) method [53] for fluid-structure interactions. The spherobot was immersed in a fluid that occupied a finite cell with no-slip walls. The visualization and analysis of the flow fields was done in VisIt [54]. Further details on the model and method are given in the Supplemental Material (SM) [55].

The swimming velocity of the spherobot was measured after steady state had been reached and was defined as the net displacement of the spherobot center of mass over one cycle. We defined the Reynolds number as $\mathrm{Re} = A_r r/\delta^2 = A_r r\omega/\nu$ because, as we will show, it is the ratio that determines the transition between small-sphere-leading and large-sphere-leading regimes; $\delta = \sqrt{\nu/\omega}$ is the oscillatory boundary layer thickness and ν is the kinematic viscosity of the fluid. We carried out simulations in two and three dimensions (2D and 3D) and found qualitative agreement. We focused on 2D because it allowed us to study a much broader parameter space. The range studied in Re was $0.001 \leqslant \mathrm{Re} \leqslant 150$. All other parameter ranges (amplitude, radii, etc.) are shown in the SM, Table S1 [55].

Results. We initially placed the spherobot in the simulation box at constant A, A_R, A_r, d_0, f, R, and r. We varied the Re via the kinematic viscosity ν. As a validation, we ran a simulation at $\mathrm{Re} = 0$ and confirmed that the spherobot did not swim (no net displacement) because of Purcell's theorem for reciprocal swimmers [48]. As soon as $\mathrm{Re} > 0$ (lowest value $\mathrm{Re} = 0.001$), the spherobot began to swim in the direction of the small sphere (Fig. 2), i.e., the small-sphere-leading regime. As Re increased, the speed of the spherobot increased until reaching a maximum at $\mathrm{Re} \approx 2$. Above $\mathrm{Re} \approx 2$ the spherobot slowed down and eventually had no net displacement (even though the spheres oscillated) at $\mathrm{Re} \approx 20$. As Re increased further, the spherobot switched direction to swim with the large sphere on the front, i.e., the large-sphere-leading regime, where its increasing speed started to plateau as Re increased further. We then ran a broader parameter sweep varying R, r, A, A_R, A_r, and d_0 in addition to the viscosity ν. We found that the transition only depended on the small sphere's radius and amplitude (in addition to viscosity) and that it was independent of all the other length scales R, A_R, and d_0. The transition-point data collapsed (within the scatter on a single, critical dimensionless number $\mathrm{Re} = A_r r/\delta^2 \approx 20$) (Fig. 2).

To gain insight into the propulsion mechanism and the switch in swimming direction, we turned our attention to the flow fields generated by the spherobot. Based on classical work on steady streaming generated by a single oscillating sphere, we expected each sphere of the spherobot to generate SS flows, which are time-averaged flows by definition. We also anticipated the SS flows around the spherobot to be different than the classical SS flows around a sphere for two reasons. First, the small sphere's oscillation amplitude A_r was of the same order of magnitude as the sphere radius, i.e., $\epsilon = A_r/r \approx O(1)$, unlike the assumption for classical steady streaming in which $\epsilon \ll 1$ [36,37,56]. Second, it was unclear what the cumulative SS flows of two spheres oscillating in antiphase should be, as it has only been studied for spheres and cylinders in phase [41,57–59]. Bearing these considerations in mind, we calculated the time-averaged flow fields around the spherobot, varying the same parameters as before (Fig. 2). We found that the switch in the swimming direction at $\mathrm{Re} \approx 20$ corresponded to the reversal of the SS flows both parallel and perpendicular to the axis of oscillation. Specifically, in the small-sphere-leading regime ($\mathrm{Re} < 20$), the fluid, on average, was pulled in towards the spheres along the axis of oscillation and was pushed out away from the spheres along the axis perpendicular to the oscillation [Fig. 3(a)]. On the contrary, in the large-sphere-leading regime ($\mathrm{Re} > 20$), the fluid, on average, did the opposite—it was pushed away from the spheres along the direction of swimming (with a strong downward jet below the small sphere) and was pulled in towards the gap between the spheres in the direction perpendicular to swimming [Fig. 3(b)].

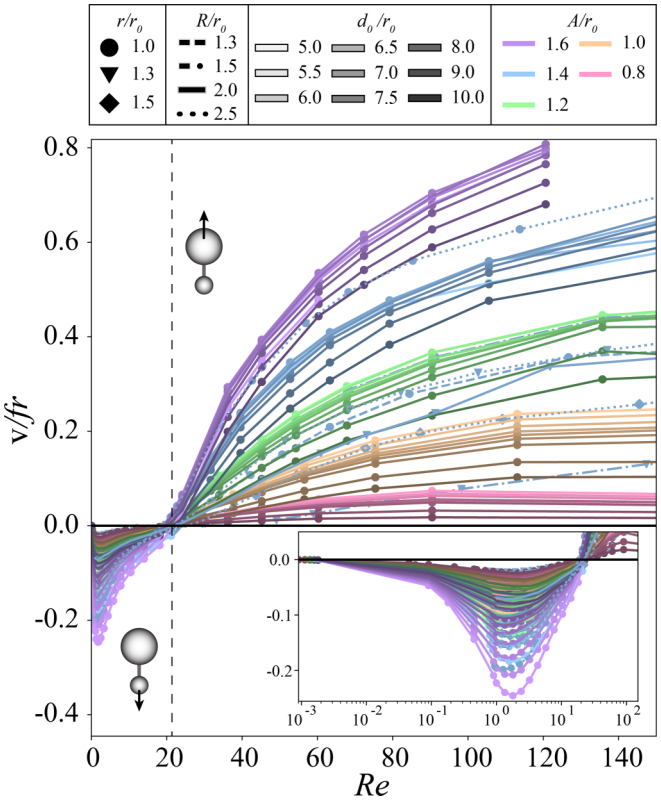

FIG. 2. Velocity of the spherobot as a function of Re in 2D for the range of A, d_0, R, and r shown in the legend. The inset shows the small-sphere-leading regime plotted on a semilogarithmic x scale. Parameters A, d_0, R, and r are nondimensionalized by the length scale, $r_0 = 0.15$ m, the radius for the small sphere. Line color indicates A, line saturation indicates d_0, line style indicates R, and symbols indicate r. Negative velocity indicates swimming in the direction of the small sphere, and positive velocity indicates swimming in the direction of the large sphere. Vertical dashed lines denote critical Re for the transition.

Furthermore, in both regimes it is clear that the velocity vectors along the oscillation axis are larger around the small sphere than the large sphere (Fig. 3). In fact, through control volume analysis, we found that for both regimes, the momentum flux on the side of the small sphere was larger than the momentum flux on the side of the large sphere (the ones along the perpendicular axis generated fluxes that canceled each other). Though initially unexpected, this finding makes sense together with the collapse, which depends on the Re of the small sphere only (Fig. 2). The net momentum flux of course switches direction as the swimming direction switches (see Fig. S4 [55]). Our data, thus, strongly suggest that the transition in the spherobot's swimming direction results from the SS flows, and this reversal is associated with the change in the direction of the net momentum flux [55].

Discussion. To better understand the reversal of SS flows, we will consider what is known for one sphere. Analytic solutions have been obtained under the small-amplitude assumption $A_r \ll r$ and in the two limiting cases relating the sphere radius to the boundary layer thickness, $\delta \gg r$ and $\delta \ll r$. The two limiting cases demonstrate a reversal in direction, shown schematically in Figs. 3(c) and 3(e) [36,37,56]. In the first case, the boundary layer thickness is much larger than the radius, $\delta \gg r$ [Fig. 3(c)]. By symmetry, we consider only one quadrant of flow. A single vortex that is the boundary layer is generated near the surface of the sphere, which pulls fluid along the axis of

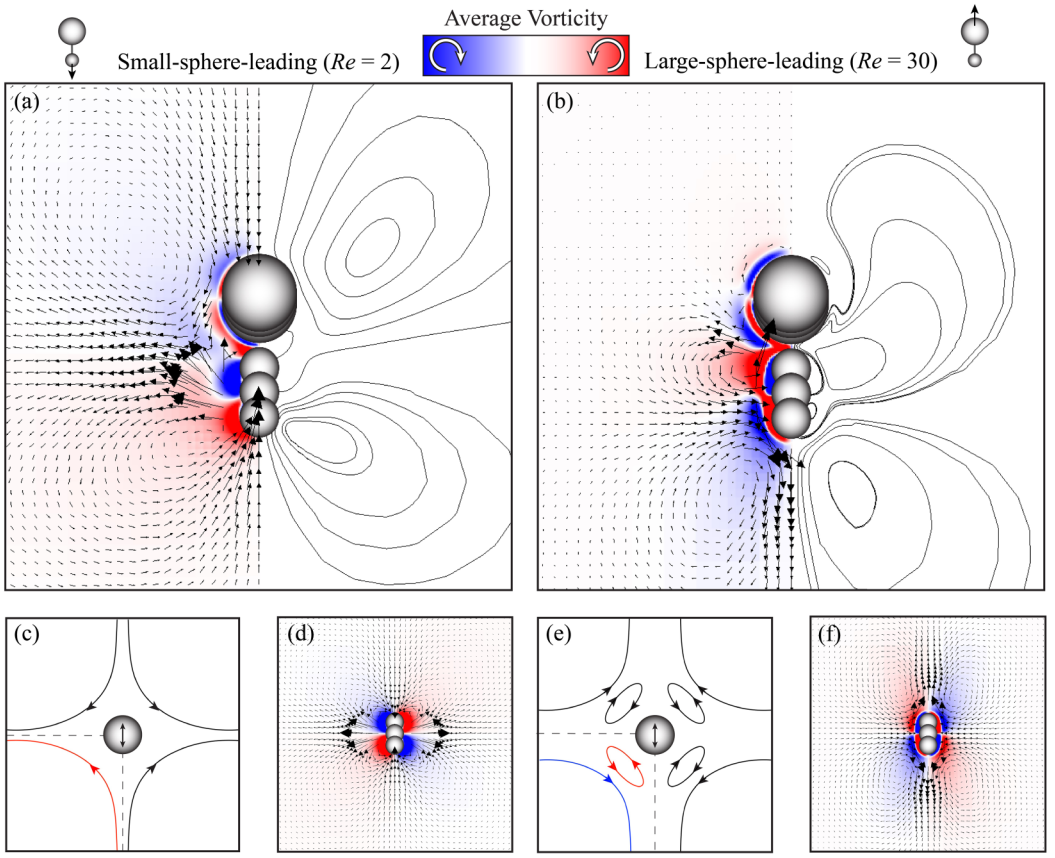

FIG. 3. Left column: Small-sphere-leading regime at Re = 2. Right column: Large-sphere-leading regime at Re = 30. Spherobot velocity field superimposed with the vorticity field and streamlines in (a) the small-sphere-leading regime and (b) the large-sphere-leading regime. The largest dimensionless velocity magnitude in (a), (b) is $|\mathbf{v}_{\max}|/fr = 0.88$. Schematic diagrams showing the reversal of steady streaming flows for one sphere in the limiting cases (c) $\delta \gg r$, and (e) $\delta \ll r$. Due to symmetry, the lower left quadrant is indicated with a dashed line. Velocity vector plot superimposed with the vorticity field for one sphere at (d) Re = 2 and (f) Re = 30. The largest dimensionless velocity magnitude in (d), (f) is $|\mathbf{v}_{\max}|/fr = 1.1$.

oscillation and pushes fluid out in the perpendicular. In the second case, the boundary layer thickness is much smaller than the radius of the sphere, $\delta \ll r$ [Fig. 3(e)]. Two vortices are generated swirling in opposite directions. The boundary layer is confined into an inner vortex close to the surface of the sphere (same direction as in the first case) but there is an additional outer vortex in the opposite direction—it pushes fluid out along the axis of oscillation and pulls it in along the perpendicular. The analytical limiting solutions that we just described provide us with a qualitative picture; we cannot use them for a direct comparison because neither $A_r \ll r$ nor $\delta \gg r$ or $\delta \ll r$ hold true for our system. Instead, we compare our results to experiments and simulations that have similar parameters to the spherobot, i.e., $\epsilon = A_r/r = O(1)$ and $r/\delta = O(1)$.

Unlike the spherobot where the reversal of flows corresponds to a switch in the direction of swimming, the point where reversal of flows occurs for a single sphere is not well defined [36,38,60,61]. Experimental studies have indicated that the inner vortex can be observed for $r/\delta \leqslant 4$ [62], whereas both experiments and simulations indicate the coexistence of inner and outer vortices with opposing flows for $r/\delta \geqslant 7$ [62–66]. It was also shown that the reversal of flows depends on the sphere's amplitude, yet a specific scaling was not found [38,60–62]. Relating all this back to

the spherobot, our data collapse gave $\mathrm{Re} = A_r r/\delta^2$ as the critical parameter for the transition in the swimming direction, a scaling that includes an amplitude dependence, as suggested by previous work [38,41,43,44,60–62]. Moreover, we found that when plotting the dimensionless velocity of the spherobot as a function of r/δ, the transition in swimming ($\mathrm{Re} \approx 20$) occurred in the range $r/\delta \approx [3.5, 7]$ (see Fig. S7 [55]), again in agreement with previous reports on the reversal of SS flows for a sphere.

We can make an analogy that the large sphere of the spherobot acts as the body of the swimmer while the small sphere acts as the flagellum. In fact, it is interesting that the SS flows, which are unrelated to the squirmer models, in the small-sphere-leading regime resemble the flow field of Stokesian pullers and in the large-sphere-leading regime resemble the flow field of Stokesian pushers [67–69]. However, the organisms that swim as pullers and pushers such as algae and bacteria, respectively, have different appendages that are responsible for "pulling" and "pushing." What is remarkable here is that the geometry of the spherobot does not have to change—the small sphere can act as an effective flagellum that can both "pull" and "push" depending only on the critical parameter $\mathrm{Re} = A_r r/\delta^2$. For example, our swimmer can switch its swimming direction by only changing its displacement amplitude.

To conclude, we have proposed a model spherobot swimmer that utilizes SS to propel itself. The main findings of the current Rapid Communication are (i) a transition in the swimming direction that collapses onto a single critical Reynolds number and (ii) the physical mechanism for the transition in swimming is the reversal of SS flows. Based on our findings, we propose that SS can be an important physical mechanism present more generally in motility at $\mathrm{Re}_{\mathrm{int}}$ both in biological organisms and also when designing artificial swimmers [45,47,70,71]. Finally, we expect to find interesting emergent collective behavior of multiple spherobot swimmers as nonlinearities accumulate leading to different steady states and patterns.

Acknowledgments. D.K. and T.D. acknowledge the National Science Foundation, Grant Award No. DMR-1753148. B.E.G acknowledges the National Science Foundation, Grant Award Nos. DMS-1410873, OAC-1450327, and DMS-1664645. A.P.S.B. acknowledges research funding from the Department of Mechanical Engineering, San Diego State University.

[1] W. Nachtigall, Some aspects of Reynolds number effects in animals, Math. Methods Appl. Sci. **24**, 1401 (2001).
[2] S. Vogel, *Life's Devices* (Princeton University Press, Princeton, NJ, 1988).
[3] S. Vogel, *Life in Moving Fluids: The Physical Biology of Flow* (Princeton University Press, Princeton, NJ, 1994), p. 467.
[4] W. Wang, W. Duan, S. Ahmed, A. Sen, and T. E. Mallouk, From one to many: Dynamic assembly and collective behavior of self-propelled colloidal motors, Acc. Chem. Res. **48**, 1938 (2015).
[5] D. Patra, S. Sengupta, W. Duan, H. Zhang, R. Pavlick, and A. Sen, Intelligent, self-powered, drug delivery systems, Nanoscale **5**, 1273 (2013).
[6] S. Tolba, R. Ammar, and S. Rajasekaran, Taking swarms to the field: A framework for underwater mission planning, in *2015 IEEE Symposium on Computers and Communication (ISCC)* (IEEE, Piscataway, NJ, 2015), pp. 1007–1013.
[7] R. Fujiwara, T. Kano, and A. Ishiguro, Self-swarming robots that exploit hydrodynamical interaction, Adv. Rob. **28**, 639 (2014).
[8] M. Duarte, V. Costa, J. Gomes, T. Rodrigues, F. Silva, S. M. Oliveira, and A. L. Christensen, Evolution of collective behaviors for a real swarm of aquatic surface robots, PloS One **11**, e0151834 (2016).
[9] S. Childress, *Mechanics of Swimming and Flying* (Cambridge University Press, Cambridge, UK, 1981).
[10] E. Lauga and T. R. Powers, The hydrodynamics of swimming microorganisms, Rep. Prog. Phys. **72**, 096601 (2009).

[11] I. K. Bartol, P. S. Krueger, W. J. Stewart, and J. T. Thompson, Pulsed jet dynamics of squid hatchlings at intermediate Reynolds numbers, J. Exp. Biol. **212**, 1506 (2009).
[12] G. Herschlag and L. Miller, Reynolds number limits for jet propulsion: A numerical study of simplified jellyfish, J. Theor. Biol. **285**, 84 (2011).
[13] S. Kern and P. Koumoutsakos, Simulations of optimized anguilliform swimming, J. Exp. Biol. **209**, 4841 (2006).
[14] L. A. Fuiman and P. W. Webb, Ontogeny of routine swimming activity and performance in zebra danios (Teleostei: Cyprinidae), Anim. Behav. **36**, 250 (1988).
[15] J. Sznitman, X. Shen, R. Sznitman, and P. E. Arratia, Propulsive force measurements and flow behavior of undulatory swimmers at low Reynolds number, Phys. Fluids **22**, 121901 (2010).
[16] M. J. McHenry, E. Azizi, and J. A. Strother, The hydrodynamics of locomotion at intermediate Reynolds numbers: Undulatory swimming in ascidian larvae (Botrylloides sp.), J. Exp. Biol. **206**, 327 (2003).
[17] A. P. S. Bhalla, B. E. Griffith, and N. A. Patankar, A forced damped oscillation framework for undulatory swimming provides new insights into how propulsion arises in active and passive swimming, PLoS Comput. Biol. **9**, e1003097 (2013).
[18] J. R. Strickler, Swimming of planktonic Cyclops species (Copepoda, Crustacea): Pattern, movements and their control, in *Swimming and Flying in Nature* (Springer, Berlin, 1975), pp. 599–613.
[19] R. W. Blake, Hydrodynamics of swimming in the water boatman, Cenocorixa bifida, Can. J. Zool. **64**, 1606 (1986).
[20] B. J. Borrell, J. A. Goldbogen, and R. Dudley, Aquatic wing flapping at low Reynolds numbers: Swimming kinematics of the Antarctic pteropod, Clione antarctica, J. Exp. Biol. **208**, 2939 (2005).
[21] B. J. Gemmell, H. Jiang, and E. J. Buskey, A tale of the ciliate tail: Investigation into the adaptive significance of this sub-cellular structure, Proc. R. Soc. B **282**, 20150770 (2015).
[22] H. Jiang, Why does the jumping ciliate Mesodinium rubrum possess an equatorially located propulsive ciliary belt? J. Plankton Res. **33**, 998 (2011).
[23] E. Kunze, J. F. Dower, I. Beveridge, R. Dewey, and K. P. Bartlett, Observations of biologically generated turbulence in a coastal inlet, Science **313**, 1768 (2006).
[24] M. M. Wilhelmus and J. O. Dabiri, Observations of large-scale fluid transport by laser-guided plankton aggregations, Phys. Fluids **26**, 101302 (2014).
[25] J. C. Nawroth and J. O. Dabiri, Induced drift by a self-propelled swimmer at intermediate Reynolds numbers, Phys. Fluids **26**, 091108 (2014).
[26] I. A. Houghton, J. R. Koseff, S. G. Monismith, and J. O. Dabiri, Vertically migrating swimmers generate aggregation-scale eddies in a stratified column, Nature (London) **556**, 497 (2018).
[27] N. G. Chisholm and A. S. Khair, Partial drift volume due to a self-propelled swimmer, Phys. Rev. Fluids **3**, 014501 (2018).
[28] S. K. Jones, Y. J. J. Yun, T. L. Hedrick, B. E. Griffith, and L. A. Miller, Bristles reduce the force required to fling wings apart in the smallest insects, J. Exp. Biol. **219**, 3759 (2016).
[29] E. Lauga, Continuous breakdown of Purcell's scallop theorem with inertia, Phys. Fluids **19**, 061703 (2007).
[30] S. Wang and A. Ardekani, Inertial squirmer, Phys. Fluids **24**, 101902 (2012).
[31] A. S. Khair and N. G. Chisholm, Expansions at small Reynolds numbers for the locomotion of a spherical squirmer, Phys. Fluids **26**, 011902 (2014).
[32] N. G. Chisholm, D. Legendre, E. Lauga, and A. S. Khair, A squirmer across Reynolds numbers, J. Fluid Mech. **796**, 233 (2016).
[33] G. Li, A. Ostace, and A. M. Ardekani, Hydrodynamic interaction of swimming organisms in an inertial regime, Phys. Rev. E **94**, 053104 (2016).
[34] J. Zhang, N.-S. Liu, and X.-Y. Lu, Locomotion of a passively flapping flat plate, J. Fluid Mech. **659**, 43 (2010).
[35] S. E. Spagnolie, L. Moret, M. J. Shelley, and J. Zhang, Surprising behaviors in flapping locomotion with passive pitching, Phys. Fluids **22**, 041903 (2010).
[36] N. Riley, On a sphere oscillating in a viscous fluid, Q. J. Mech. Appl. Math. **19**, 461 (1966).
[37] N. Riley, Steady streaming, Annu. Rev. Fluid Mech. **33**, 43 (2001).

[38] E. J. Chang and M. R. Maxey, Unsteady flow about a sphere at low to moderate Reynolds number. Part 1. Oscillatory motion, J. Fluid Mech. **277**, 347 (1994).
[39] C. W. Kotas, M. Yoda, and P. H. Rogers, Visualization of steady streaming near oscillating spheroids, Exp. Fluids **42**, 111 (2007).
[40] F. Otto, E. K. Riegler, and G. A. Voth, Measurements of the steady streaming flow around oscillating spheres using three dimensional particle tracking velocimetry, Phys. Fluids **20**, 093304 (2008).
[41] D. Klotsa, M. R. Swift, R. M. Bowley, and P. J. King, Interaction of spheres in oscillatory fluid flows, Phys. Rev. E **76**, 056314 (2007).
[42] H. S. Wright, M. R. Swift, and P. J. King, Migration of an asymmetric dimer in oscillatory fluid flow, Phys. Rev. E **78**, 036311 (2008).
[43] D. Klotsa, M. R. Swift, R. M. Bowley, and P. J. King, Chain formation of spheres in oscillatory fluid flows, Phys. Rev. E **79**, 021302 (2009).
[44] D. Klotsa, K. A. Baldwin, R. J. A. Hill, R. M. Bowley, and M. R. Swift, Propulsion of a Two-Sphere Swimmer, Phys. Rev. Lett. **115**, 248102 (2015).
[45] T. A. Spelman and E. Lauga, Arbitrary axisymmetric steady streaming: Flow, force and propulsion, J. Eng. Math. **105**, 31 (2017).
[46] B. R. Lutz, J. Chen, and D. T. Schwartz, Hydrodynamic tweezers: 1. Noncontact trapping of single cells using steady streaming microeddies, Anal. Chem. **78**, 5429 (2006).
[47] K. M. Ehlers and J. Koiller, Could cell membranes produce acoustic streaming? Making the case for synechococcus self-propulsion, Math. Comput. Modell. **53**, 1489 (2011).
[48] E. M. Purcell, Life at low Reynolds number, Am. J. Phys. **45**, 3 (1977).
[49] B. Kallemov, A. P. S. Bhalla, B. E. Griffith, and A. Donev, An immersed boundary method for rigid bodies, Commun. Appl. Math. Comput. Sci. **11**, 79 (2016).
[50] F. Balboa Usabiaga, B. Kallemov, B. Delmotte, A. P. S. Bhalla, B. E. Griffith, and A. Donev, Hydrodynamics of suspensions of passive and active rigid particles: A rigid multiblob approach, Commun. Appl. Math. Comput. Sci. **11**, 217 (2016).
[51] B. E. Griffith, R. D. Hornung, D. M. McQueen, and C. S. Peskin, An adaptive, formally second order accurate version of the immersed boundary method, J. Comput. Phys. **223**, 10 (2007).
[52] IBAMR: An adaptive and distributed-memory parallel implementation of the immersed boundary method, https://github.com/IBAMR/IBAMR
[53] C. S. Peskin, The immersed boundary method, Acta Numerica **11**, 479 (2002).
[54] H. Childs, E. Brugger, B. Whitlock, J. Meredith, S. Ahern, D. Pugmire, K. Biagas, M. Miller, C. Harrison, G. H. Weber, H. Krishnan, T. Fogal, A. Sanderson, C. Garth, E. W. Bethel, D. Camp, O. Rübel, M. Durant, J. M. Favre, and P. Navrátil, VisIt: An end-user tool for visualizing and analyzing very large data, in *High Performance Visualization-Enabling Extreme-Scale Scientific Insight*, edited by E. W. Bethel, H. Childs, and C. Hansen (CRC Press, Boca Raton, FL, 2012), pp. 357–372.
[55] See Supplemental Material at http://link.aps.org/supplemental/10.1103/PhysRevFluids.4.021101 for more details on methods, additional figures, and movies of the spherobot.
[56] J. M. Andres and U. Ingard, Acoustic streaming at low Reynolds numbers, J. Acoust. Soc. Am. **25**, 932 (1953).
[57] Z. Zapryanov, Zh. Kozhoukharova, and A. Iordanova, On the hydrodynamic interaction of two circular cylinders oscillating in a viscous fluid, Z. Angew. Math. Phys. (ZAMP) **39**, 204 (1988).
[58] S. S. Tabakova and Z. D. Zapryanov, On the hydrodynamic interaction of two spheres oscillating in a viscous fluid. I. Axisymmetrical case, Z. Angew. Math. Phys. (ZAMP) **33**, 344 (1982).
[59] S. S. Tabakova and Z. D. Zapryanov, On the hydrodynamic interaction of two spheres oscillating in a viscous fluid. II. Three dimensional case, Z. Angew. Math. Phys. (ZAMP) **33**, 487 (1982).
[60] R. S. Alassar and H. M. Badr, Oscillating viscous flow over a sphere, Comput. Fluids **26**, 661 (1997).
[61] H. M. Blackburn, Mass and momentum transport from a sphere in steady and oscillatory flows, Phys. Fluids **14**, 3997 (2002).
[62] M. Tatsuno, Circulatory streaming around an oscillating circular cylinder at low Reynolds numbers, J. Phys. Soc. Jpn. **35**, 915 (1973).
[63] W. Coenen and N. Riley, Oscillatory flow about a cylinder pair, Q. J. Mech. Appl. Math. **62**, 53 (2008).

[64] M. Tatsuno, Secondary flow induced by a circular cylinder performing unharmonic oscillations, J. Phys. Soc. Jpn. **50**, 330 (1981).
[65] T. Olsen, Rotational flow of a viscous fluid, J. Acoust. Soc. Am. **28**, 313 (1956).
[66] J. Holtsmark, I. Johnsen, T. Sikkeland, and S. Skavlem, Boundary layer flow near a cylindrical obstacle in an oscillating, incompressible fluid, J. Acoust. Soc. Am. **26**, 26 (1954).
[67] M. J. Lighthill, On the squirming motion of nearly spherical deformable bodies through liquids at very small Reynolds numbers, Commun. Pure Appl. Math. **5**, 109 (1952).
[68] J. R. Blake, A spherical envelope approach to ciliary propulsion, J. Fluid Mech. **46**, 199 (1971).
[69] T. J. Pedley, Spherical squirmers: models for swimming micro-organisms, IMA J. Appl. Math. **81**, 488 (2016).
[70] K. Ehlers and J. Koiller, Synechococcus as a "singing" bacterium: Biology inspired by micro-engineered acoustic streaming devices, arXiv:0903.3781.
[71] F. Nadal and E. Lauga, Asymmetric steady streaming as a mechanism for acoustic propulsion of rigid bodies, Phys. Fluids **26**, 082001 (2014).